LA-UR 96-1635 CONF-960810--1

Los Alamos National Laboratory is operated by the University of California for the United States Department of Energy under contract W-7405-ENG-36

TITLE: A SEMI-EULERIAN METHOD FOR TREATING LAGRANGIAN SLIDING INTERFACES

AUTHOR(S): WEN HO LEE, XHM

SUBMITTED TO: THE THIRD INTERNATIONAL CONFERENCE ON COMPUTATIONAL STRUCTURES TECHNOLOGY,
21-23 AUGUST 1996,
BUDAPEST, HUNGARY

Los Alamos National Laboratory
Los Alamos, New Mexico 87545

A SEMI-EULERIAN METHOD FOR TREATING LAGRANGIAN SLIDING INTERFACES

Wen Ho Lee
University of California
Los Alamos National Laboratory
Los Alamos, NM 87545 USA

ABSTRACT

In many two-dimensional Lagrangian radiation hydrodynamic calculations, shear along material boundaries is a serious problem. Since the mesh is tied to the material, this shear will cause distortions in the mesh that make the calculations very difficult. The approach described in this paper adopts a semi-Eulerian calculation that allows material flow through a Lagrangian mesh along an interface. The basic idea is to consider each point along the slip line temporarily as a double point. One would then calculate the motion of each point separately and then pull the points back together using the automatic rezone method. This would allow the materials to shear along the interface. This paper will describe the method as used in a two-dimensional Lagrangian code. The formation of a shaped charge jet is computed using the present method, and the results are discussed with and without the slip treatment. A nonsymmetric radiation-driven shock problem is also shown.

1 INTRODUCTION

In many two-dimensional Lagrangian radiation hydrodynamic calculations, shear along material boundaries is a serious problem. Since the mesh is tied to the material, this shear will cause distortions in the mesh that make the calculations very difficult. What is needed to handle this situation is a method of allowing material flow along interfaces.

A number of methods have been implemented to try to take care of this problem. One of the most successful of these methods for hydrodynamic calculations has been to turn the interface into two lines in the mesh that move semi-independently. However, this method makes it necessary to use some approximations at the interface for computing special physics; for example, the radiation hydrodynamic coupling problems.

The approach described in this paper adopts a semi-Eulerian calculation that allows material flow through a Lagrangian mesh along an interface. It is not necessary to have any special mesh, and all calculations, other than the hydrodynamics, are unchanged. The basic idea is to consider each point along the slip line temporarily as a double point. One would then calculate the motion of each point separately and then pull the points back together using the automatic rezone method [1]. This would allow the materials to shear along the interface.

This paper will describe the method as used in a two-dimensional Lagrangian code. The formation of a shaped charge jet is computed using the present method and the results are discussed with and without the slip treatment. A nonsymmetric radiation-driven shock problem is also shown.

2 GENERAL DESCRIPTION OF THE METHOD

In a true Lagrangian code, the molecules near a boundary in one zone are effectively tied to the molecules near that same boundary in the adjacent zone. Zones along an interface cannot slide or slip with respect to each other even if such slip were physically desirable or realistic. The purpose of the slip code is to allow these two materials to slip with respect to each other.

In the logical domain, we use ℓ and k lines to represent the zone boundary. Since the method for treating the ℓ line slip is the same as for k line. We like to describe the slip along the ℓ line only.

First, we consider the slip interface as having two additional mass points: one associated with the two zone masses above the interface and the other with the two zone masses below the interface. We calculate the velocities of these two assumed points separately by using a modified form of the Schulz [2] hydrodynamic equations.

If we refer to Schulz's Report UCRL-6776 [3], pp 28-29 (also see Appendix A of this paper for more detailed derivation) where he gives his acceleration equations; we see that at each node he has 4 terms (see Fig. 1), each weighted by a η or ξ which are derived from the spacing (see Eq. (A-24) and (A-25)). In Fig. 1, let us take the line $\ell = \ell$ (for $k = k-1, k$, and $k+1$) as the slip line. We temporarily assume that point $G(k,\ell)$ is two points (above and below ℓ). We calculate an acceleration, velocity, and position above ℓ and below ℓ. Then we pull the two positions back together with the rezone technique to form a single point. The mesh will be moved through the material allowing the materials on both sides of the line to move with respect to each other. We will leave the new velocities above ℓ and below ℓ as they are. After the rezone, an appropriate velocity for the single point will be formed for the use in the normal code computation.

For the above ℓ calculation, we drop out the first term on the right-hand side of Eq. (A-27) altogether (see Fig. 2), i.e., $\eta_{k,\ell} = 0$. Since $\eta_{k,\ell} = 0$, we have the coefficient of the third term equal to 2. The coefficients of the 2nd and 4th terms are unchanged. Therefore, Eq. (A-27) becomes

$$D\bar{u}^n_{k,\ell} =$$

$$Dt^n \left\{ -\xi_{k,\ell} \left[\frac{\partial \bar{\bar{R}} / \partial k}{2\rho j} \frac{\partial_2 P}{\partial \ell} + \frac{1}{2M} \frac{\partial}{\partial \ell} \left(\hat{R} \frac{\partial \bar{\bar{R}}}{\partial k} 2 q_B \right) \right]^n_{k-\frac{1}{2},\ell} \right.$$

$$+2 \left[\frac{\partial \bar{\bar{R}} / \partial \ell}{2\rho j} \frac{\partial_3 P}{\partial k} + \frac{1}{2M} \frac{\partial}{\partial k} \left(\hat{R} \frac{\partial \bar{\bar{R}}}{\partial \ell} 3 q_A \right) \right]^n_{k,\ell+\frac{1}{2}}$$

$$\left. -\left(2 - \xi_{k,\ell}\right) \left[\frac{\partial \bar{\bar{R}} / \partial k}{2\rho j} \frac{\partial_4 P}{\partial \ell} + \frac{1}{2M} \frac{\partial}{\partial \ell} \left(\hat{R} \frac{\partial \bar{\bar{R}}}{\partial k} 4 q_B \right) \right]^n_{k+\frac{1}{2},\ell} \right\}$$

(1)

For the below ℓ calculation, we drop out the third term on the right-hand side of Eq. (A-27) altogether, i.e., make $2 - \eta_{k,\ell} =$ or $\eta_{k,\ell} = 2$; again the coefficients of the 2nd and 4th terms are unchanged. Therefore, Eq. (A-27) becomes

$$D\bar{u}^n_{k,\ell} = Dt^n \left\{ 2 \left[\frac{\partial \bar{\bar{R}} / \partial \ell}{2\rho j} \frac{\partial_1 P}{\partial k} + \frac{1}{2M} \frac{\partial}{\partial k} \left(\hat{R} \frac{\partial \bar{\bar{R}}}{\partial \ell} 1 q_A \right) \right]^n_{k,\ell-\frac{1}{2}} \right.$$

$$-\xi_{k,\ell} \left[\frac{\partial \bar{\bar{R}} / \partial \ell}{2\rho j} \frac{\partial_2 P}{\partial k} + \frac{1}{2M} \frac{\partial}{\partial \ell} \left(\hat{R} \frac{\partial \bar{\bar{R}}}{\partial k} 2 q_B \right) \right]^n_{k-\frac{1}{2},\ell}$$

$$\left. -\left(2 - \xi_{k,\ell}\right) \left[\frac{\partial \bar{\bar{R}} / \partial k}{2\rho j} \frac{\partial_4 P}{\partial \ell} + \frac{1}{2M} \frac{\partial}{\partial \ell} \left(\hat{R} \frac{\partial \bar{\bar{R}}}{\partial k} 4 q_B \right) \right]^n_{k+\frac{1}{2},\ell} \right\}$$

(2)

The results are shown in Fig. 3. In calculating the momentum equations, we use term 3 as they would be used in non-slip calculations. This choice is important because it means that the pressures in material B affect the velocities in material A and vice versa. Consequently, the separate accelerations are not completely independent. However we are allowing the two sets of mass to move differently, if they are so inclined, because different accelerations applied to two points with the same position will give different velocities and hence different new positions. Using the result of Eq. (1), we can get the new velocity vector at time $n + \frac{1}{2}$ from

$$\bar{u}^{n+\frac{1}{2}}_{k,\ell} = \bar{u}^{n-\frac{1}{2}}_{k,\ell} + D\bar{u}^n_{k,\ell} \tag{3}$$

where

$$\bar{u}^{n+\frac{1}{2}}_{k,\ell} = \begin{pmatrix} u^{n-\frac{1}{2}}_{k,\ell} & , & v^{n+\frac{1}{2}}_{k,\ell} \end{pmatrix} \tag{4}$$

The new location S for the above ℓ zones (See Fig. 4) is computed from

$$\bar{R}^{n+1}_{k,\ell} = \left(R^n_{k,\ell} + Dt^{n+\frac{1}{2}} u^{n+\frac{1}{2}}_{k,\ell} \quad , \quad Z^n + Dt^{n+\frac{1}{2}} v^{n+\frac{1}{2}}_{k,\ell} \right) \tag{5}$$

and the new location W for the below ℓ zones is obtained by using Eqs. (2), (3), (4), and (5). Fig. 4 shows the zones along the interface after the two separate motions have been calculated. These zones may overlap, separate, etc. In the present example, as shown in Fig. 5, points S and W have penetrated into the other material. Now we have the two points in different positions. We now pick a point where they should coincide (such as the average position). There are a number of possible ways to pick this position.

Let M_5 be the mass of the zone $\overline{DHSE}$ and M_6 of the zone $\overline{HFPS}$ as shown in Fig. 5. Similarly, M_7 is the mass of the left zone below ℓ and M_8 is that of the right zone. To get the position of the coincident point N, we use the mass-weighted average of the two slip velocities. For example, the coordinates of N are

$$R^{n+1}_N = R^n_{k,\ell} + Dt^{n+\frac{1}{2}} \left(u^{n+\frac{1}{2}}_{k,\ell} \right)_{average}$$

$$Z^{n+1}_N = R^n_{k,\ell} + Dt^{n+\frac{1}{2}} \left(v^{n+\frac{1}{2}}_{k,\ell} \right)_{average}$$

where

$$\left(u^{n+\frac{1}{2}}_{k,\ell} \right)_{average} =$$

$$\left[\left(M_5 + M_6\right) \left(u^{n+\frac{1}{2}}_{k,\ell} \right)_a \left(M_7 + M_8\right) \left(u^{n+\frac{1}{2}}_{k,\ell} \right)_b \right]$$

$$/(M_5 + M_6 + M_7 + M_8)$$

and

$\left(u_{k,\ell}^{n+\frac{1}{2}}\right)_a$ is obtained from Eqs. (1), (3), and (4), while $\left(u_{k,\ell}^{n+\frac{1}{2}}\right)_b$ is from Eqs. (2), (3), and (4). $\left(v_{k,\ell}^{n+\frac{1}{2}}\right)_{average}$ is calculated similar to $\left(u_{k,\ell}^{n+\frac{1}{2}}\right)_{average}$.

Picking a coincident point, N, for the two points, S and W, defines a displacement for both of the points which is used is rezoning. We now use the rezone [1] package to move the points together with the material outside the zones treated as a vacuum. Material may transfer between zone $\overline{DHSE}$ and zone $\overline{HFPS}$ which have the same kind of material, but material in M_5 cannot move to M_7. In Fig. 5, the material in ΔHTN will be removed from M_5 and added to M_6. After the rezone calculations, the kinetic energy or the internal energy may be transferred across the material interface. The mesh line inside the zones, e.g., $\overline{HT}$, is moved through the material, leaving the material in its new position, thus allowing slip along the interface. In the resultant mesh, the temporary separation of the points is eliminated. The two velocities on the temporary points are preserved for use on the next cycle. This process is repeated for each point along the slip line. The slip along a k line is handled in a similar way.

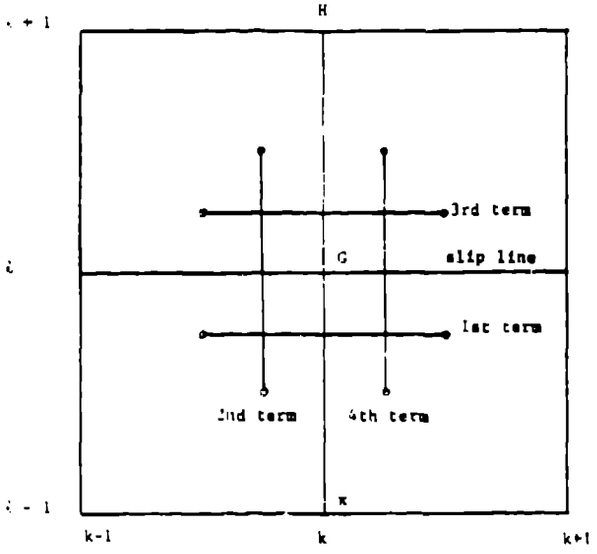

Fig. 1. The Lagrangian zones (or logical zones) with slip line along $\ell = \ell$ line. The 1st, 2nd, 3rd, and 4th terms represent the four term on the right-hand side of Eq. (A-27).

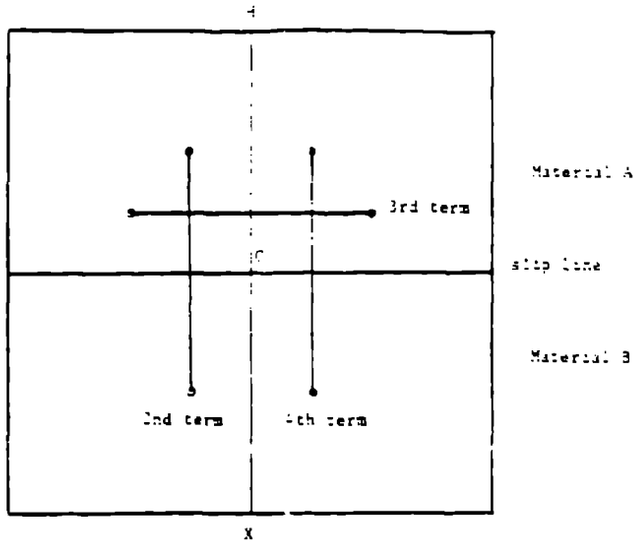

Fig. 2. Only 2nd, 3rd, and 4th terms are used for computing the momentum equation, Eq. (1), for the above ℓ calculation.

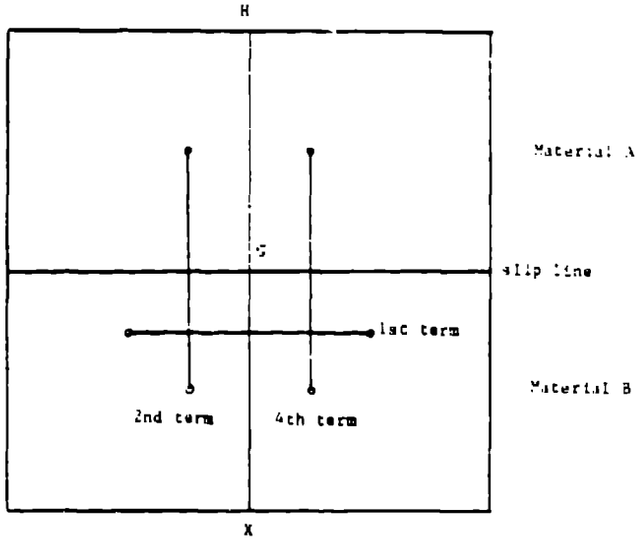

Fig. 3. Only 1st, 2nd, and 4th terms are used for computing the momentum equation, Eq. (2), for the below ℓ calculation.

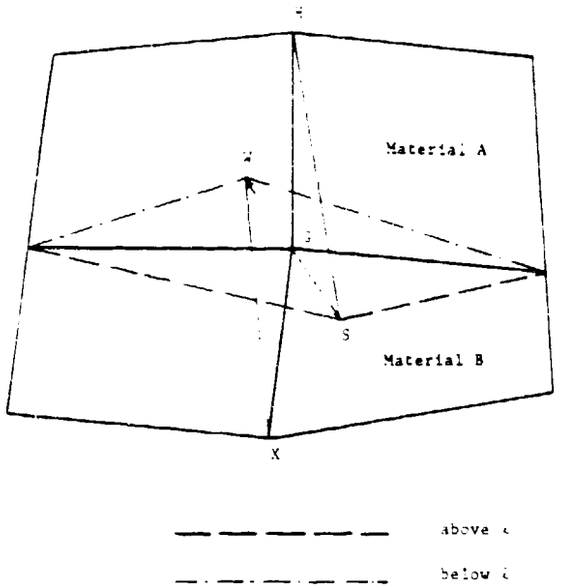

Fig. 4. Point S is the new location of G for the above ℓ calculation via Eq. (1). Similarly, the new location W is from Eq. (2) for the below ℓ calculation.

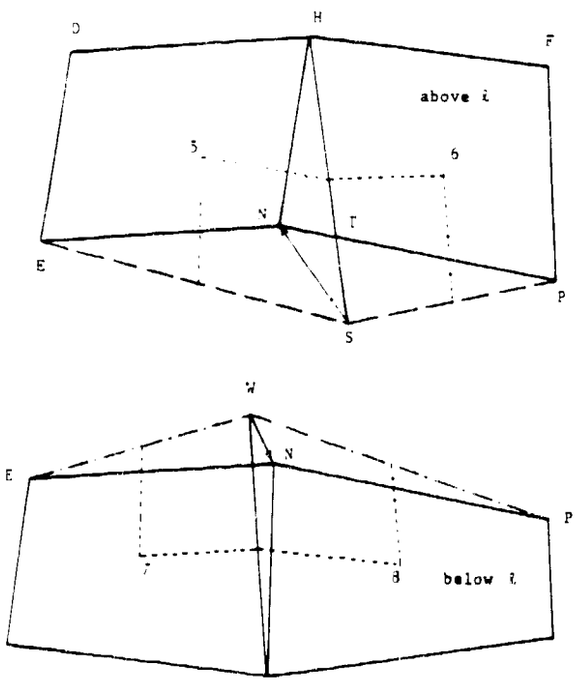

Fig. 5. The top figure is the above ℓ zones. After a mass weighting of velocities, the coincident point N is defined. Points 5 and 6 indicate the zone center of $\overline{DHSE}$ and $\overline{HFPS}$. Similar notations are used for the below ℓ zones as described in the lower figure.

3 CALCULATION OF SHAPED CHARGE PROBLEM WITH SLIP

The shaped charge used in this study is described in Fig. 6. The aluminum cone liner has an outside diameter of 6 cm and thickness of 0.7023 cm and is divided into six zones. The shaped charge is detonated with a EX-12 detonator which initiates the detonation-sheet explosive. The detonation wave in the detonation sheet propagates radially outward until it detonates the LX-14 explosive which is divided into 40 zones. The foam wave shaper prevents the detonation wave from pre-igniting the LX-14 in the interior region. This wave-shaping method changes the angle of the incidence of the detonation wave on the liner providing for an extremely high collapse and jet tip velocity. Fig. 7 shows the zoning of the current simulation including aluminum liner and LX-14 only. Due to the axisymmetry, we only model half of the problem. There are 40 zones in the radial direction and 46 zones in the axial direction. The high explosive has a ring detonation located at $R = 6$ cm and $Z = 11.529$ cm.

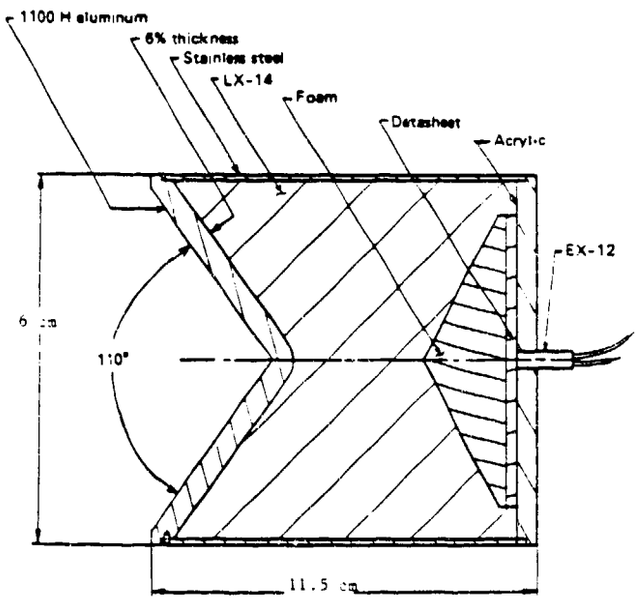

Fig. 6. Shaped charge design configuration for code calibration and verification.

Fig. 8 shows the sequence calculations at time $30\,\mu$sec and 40 μsec for both with and without slip treatment. When one uses a 2D Lagrangian code without slip for material interfaces to simulate the shaped charge problems, the zones located at the outside ring surface, i.e., $\overline{DA}$ for this problem, always present some difficulties for calculation. Part of the problem is due to the turbulent nature of burned product gas of the high explosive near the interface. Most of the existing 2D Lagrangian code for metal-explosive interaction does not include the turbulent physics or separation flow due to turbulent. The other problem is due to the lacking of slip at the material interface which results in high shearing stress inside the metal zones. This fact is observed at location $D(k = 1, \ell = 41)$ and $C(k = 1, \ell = 8)$ at time 40 μsec on the top two plots of Fig. 8. The final jet velocity and shape of the calculations with slip option is much closer to the experimental data.

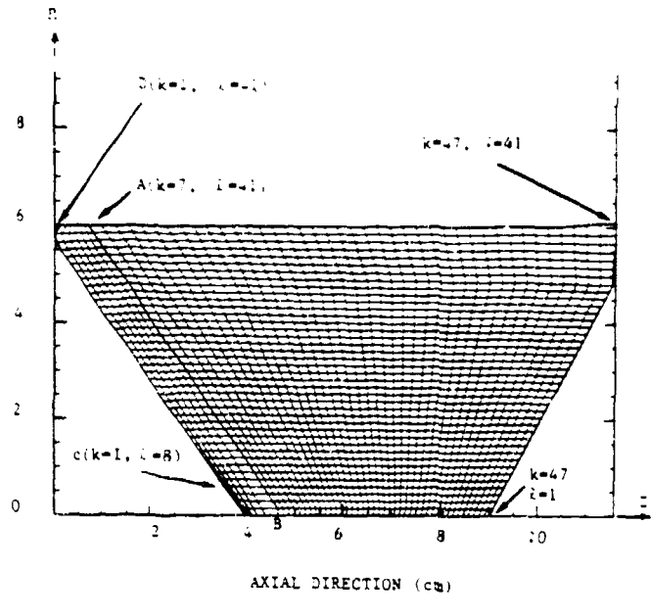

Fig. 7. The 2D Lagrangian grid at time 1 μsec with 40 zones axially in the high explosive, 6 zones axially in the aluminum liner, and 40 zones in the radial direction. The slip surface is from $A(k=7,\ell=41)$ to $B(k=7,\ell=1)$ which is also the material interface.

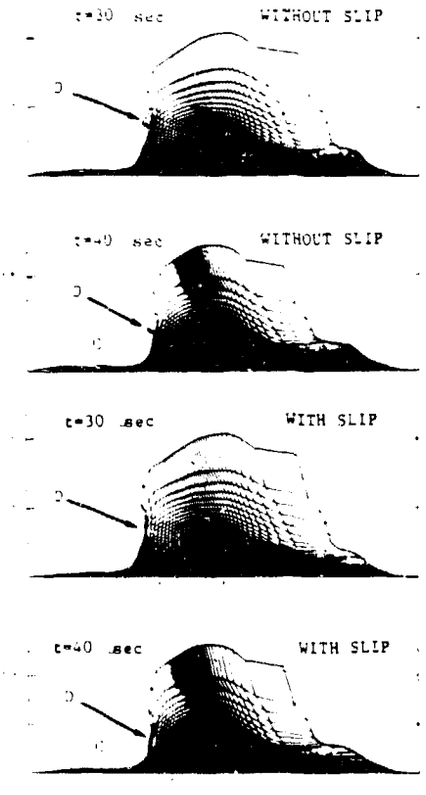

Fig. 8. The grid formation of the aluminum liner and the high explosive at time 30, and 40 μsec without slip treatment (top two plots) and with slip (bottom two plots). At time 40 μsec, the liner surfaces at $D(k=7,\ell=41)$ and $C(k=1,\ell=8)$ are much closer to the experimental data for the calculations with slip.

4 RADIATION HYDRODYNAMIC TEST PROBLEM

The initial mesh of the radiation hydrodynamic test problem is shown in Fig. 9 (Top). This problem consists of a layer of high-density material (top 5 rows) and a layer of low-density material (bottom 5 rows). The problem is driven by feeding energy into the bottom layer of low-density material to produce a nonsymmetric shock. Initial temperature is zero in the whole problem. At time $t > 0$, the temperature of the left five zones as indicated by S are set to 0.5 keV. All of the four outside boundaries are nonflow boundaries. Fig. 9 shows the mesh and velocity vectors at time 1 μsec for no slip calculation (center) and with slip at interface (bottom). The mesh with slip treatment is much better, and the velocity vectors along the interfacial grid are almost normal to the interfacial boundary.

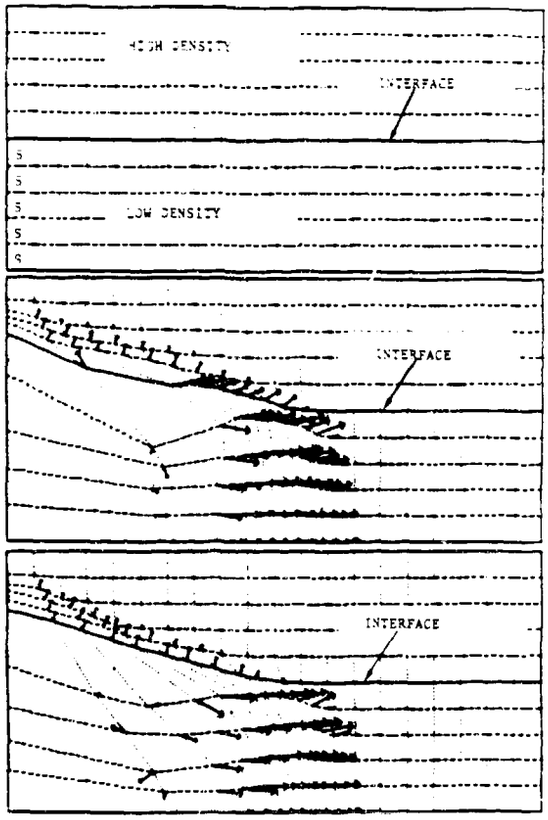

Fig. 9. Top: Initial mesh of high- and low- density materials with temperature equals zero everywhere. When $t > 0$, the temperature of the left five zones of the low density material is raised to 0.5 keV.
Center: Velocity vectors and mesh plot at 1 μsec without slip.
Bottom: Velocity vector and mesh plot at 1 μsec with slip.

5 CONCLUSIONS

Mesh distortions along the material interface for 2D Lagrangian code is a well-known problem. This situation becomes more serious when the density ratio of the different materials is high. The present method described in Section II will minimize the shearing stress along the interface and consequently make the resultant velocity vectors on the

interfacial grid nearly perpendicular to the material boundaries.

By using the present method, the total number of grids in the problem remains constant and no dislocation or separation of the grid point along the material interface will occur. This makes the computations of the radiation transport much easier. Lagrangian code is more accurate then Eulerian method for modeling small deformation problems. But for large deformation, e.g., the shaped charge problem described in Section III after time $t > 50$ μsec, one may have to use more rezone computations in order to continue the run or may have to use a Eulerian code to finish the calculations. The slip method discussed in this paper can only help the Lagrangian calculations up to a certain point.

REFERENCES

1. Wallick, K. B., "REZONE: A Method for Automatic Rezoning in Two-Dimensional Lagrangian Hydrodynamic Problems," Los Alamos National Laboratory report LA-10829-MS (1987).

2. Schulz, W. D., "Two-Dimensional Lagrangian Hydrodynamic Difference Equation," in Method in Computational Physics, Vol. 3, pp. 1-45 (1964).

3. Schulz, W. D., "Two-Dimensional Lagrangian Hydrodynamic Difference Equation," Lawrence Radiation Laboratory report UCRL-6776 (1963).

APPENDIX A

THE HYDRODYNAMIC DIFFERENCE EQUATIONS

A.1 - Definitions of *Variable* and *Notation*

In this appendix, we describe the definitions of *variable* and *notation* which will be used for the governing equations such as the conservation of mass, momentum, and energy.

A typical zone of the present computation is shown in Fig. A-1.

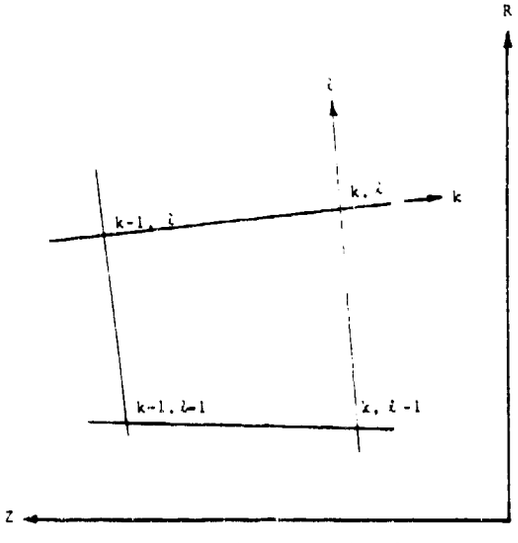

Fig. A-1. A typical computational zone.

On this mesh, we then have two types of variables—zone variables, defined at zone centers and point variables defined at mesh points. The zone variables are defined so that the mass of zone k,ℓ appears as $M_{k-\frac{1}{2},\ell-\frac{1}{2}}$ and similarly for the other zone-centered quantities. We will occasionally, for brevity, use k,ℓ instead of $k-\frac{1}{2},\ \ell-\frac{1}{2}$, and $k-1,\ell$ instead of $k-\frac{3}{2},\ell$, etc., in Fig. A-1, the following definitions hold:

$R(k,\ell,t)$= Eulerian coordinate (Cartesian or cylindrical) in cm.

$Z(k,\ell,t)$= Eulerian coordinate (always Cartesian) in cm.

$\vec{R}$= Vector (R,Z)

k= Lagrange coordinate

ℓ= Lagrange coordinate

j= Jacobian of the transformation between (R,Z) and (k,ℓ) in cm2.

Letting $R_k = \partial R/\partial k, R_\ell = \partial R/\partial \ell$, etc., then

$$j = R_k Z_\ell - R_\ell Z_k \tag{A-1}$$

Define

$$\hat{R} = \begin{cases} R & \text{for cylindrical coordinates} \\ 1 & \text{for Cartesian coordinates} \end{cases} . \tag{A-2}$$

then a volume Jacobian may be defined as

$$J = \hat{R} j \quad . \tag{A-3}$$

We now want to obtain the relations which take us from Eulerian space derivatives to their corresponding Lagrange counterparts:

$$\frac{\partial}{\partial R} = \frac{\partial k}{\partial R}\frac{\partial}{\partial k} + \frac{\partial \ell}{\partial R}\frac{\partial}{\partial \ell} \tag{A-4}$$

$$\frac{\partial}{\partial Z} = \frac{\partial k}{\partial Z}\frac{\partial}{\partial k} + \frac{\partial \ell}{\partial Z}\frac{\partial}{\partial \ell} \tag{A-5}$$

Expressions are required which relate $\partial k/\partial R \ldots \partial \ell/\partial Z$ to $R_k, \ldots Z_\ell$. For arbitrary g we have

$$\frac{\partial g}{\partial k} = R_k \frac{\partial g}{\partial R} + Z_k \frac{\partial g}{\partial Z} \quad , \tag{A-6}$$

$$\frac{\partial g}{\partial \ell} = R_\ell \frac{\partial g}{\partial R} + Z_\ell \frac{\partial g}{\partial Z} \quad . \tag{A-7}$$

Letting $g = k$ we can solve for $\partial k/\partial R$ and $\partial k/\partial Z$, and letting $g = \ell$ provides $\partial \ell/\partial R$ and $\partial \ell/\partial Z$. The result is

$$\frac{\partial k}{\partial R} = \frac{Z_\ell}{j}$$

$$\frac{\partial \ell}{\partial R} = \frac{Z_k}{j}$$

$$\frac{\partial k}{\partial Z} = \frac{R_\ell}{j} \qquad \text{(A-8)}$$

$$\frac{\partial \ell}{\partial Z} = \frac{R_k}{j}$$

which gives

$$\frac{\partial}{\partial R} = \frac{Z_\ell}{j}\frac{\partial}{\partial k} - \frac{Z_k}{j}\frac{\partial}{\partial \ell},$$

$$\frac{\partial}{\partial Z} = -\frac{R_\ell}{j}\frac{\partial}{\partial k} + \frac{R_k}{j}\frac{\partial}{\partial \ell} \quad . \qquad \text{(A-9)}$$

Now define a vector $\bar{\bar{R}}$ which lags $\bar{R}$ by 90°as the normal vector to $\bar{R}$, thus

$$\bar{\bar{R}} = (Z, -R) \quad . \qquad \text{(A-10)}$$

We now define the gradient operator in Lagrange space as $\bar{\nabla} \to \bar{D}$ where

$$\bar{D} = \frac{1}{j}\left[\bar{\bar{R}}_\ell \frac{\partial}{\partial k} - \bar{\bar{R}}_k \frac{\partial}{\partial \ell}\right] \qquad \text{(A-11)}$$

$$= \frac{1}{j}\left[\frac{\partial}{\partial k}\left(\bar{\bar{R}}_\ell \ldots\right) + \frac{\partial}{\partial \ell}\left(\bar{\bar{R}}_\ell \ldots\right)\right] \qquad \text{(A-12)}$$

Hence, for arbitrary function f and vector $\bar{f}$, we have

$$\bar{\nabla} f = \bar{D} f$$

$$\bar{\nabla} \cdot \bar{f} = \frac{1}{R}\bar{D} \cdot \left(\hat{R}\bar{f}\right) \quad . \qquad \text{(A-13)}$$

Lagrange time derivatives, i.e., partial derivatives with respect to time with k and ℓ fixed, are written as

$$u(k,\ell,t) = \frac{\partial R}{\partial t} = \dot{R} = R_t = R \text{ velocity in cm/shake}$$

$$\mathrm{v}(k,\ell,t) = \frac{\partial Z}{\partial t} = \dot{Z} = Z_t = Z \text{ velocity in cm/shake}$$

$$\bar{u} = \text{the vector } (u, \mathrm{v}) \qquad \text{(A-14)}$$

where 1 shake = 10^{-8} seconds.

In addition to the variables already defined, i.e., R, Z, u, v, which are point variables and j, a zone variable, we have the following definitions where (Z) implies a zone variable, (P) a point variable, and (I) an interface variable:

M = mass(gms) (Z)

$\tau = 1/\rho$ = specific volume (cm^2/g,) (Z)

P^m = material pressure (jerks/ cm^3) (Z)

where 1 jerk = 10^{16} ergs

E^M = material energy per unit volume (jerks/ cm^3) (Z)

ε^m = material specific energy (jerks/cm) (Z)

c_v = material specific heat at constant specific volume (jerks/gm/keV) (Z)

c = speed of light = 300 cm/shake

$I\left(\bar{r}, \nu, \bar{\Omega}, t\right)$ = specific intensity of the radiation field defined as the rate of energy flow per unit frequency and solid angle across a unit area oriented normal to the direction of propagation at point $\bar{r}$, frequency ν, in direction $\bar{\Omega}$ at time t.

$E = \frac{1}{c}\int_0^{\infty} d\nu \int_{4\pi} I\left(\nu, \bar{\Omega}\right) d\bar{\Omega}$ = radiation energy density (jerks/ cm^3) (Z)

$\bar{F} = \int_0^{\infty} d\nu \int_{4\pi} \bar{\Omega} I\left(\nu, \bar{\Omega}\right) d\bar{\Omega}$ = radiative flux (jerks/ cm^2/shake) (I)

$\bar{\bar{P}}^r = \frac{1}{c}\int_0^{\infty} d\nu \int_{4\pi} \bar{\Omega}\bar{\Omega} I\left(\nu, \bar{\Omega}\right) d\bar{\Omega}$ = radiation energy tensor (jerks/ cm^3) (Z)

$\mu_a(\nu)$ = absorption coefficient at frequency ν (cm^{-1}) (Z)

$\mu_a'(\nu) = \mu_a(\nu)\left(1 - e^{-h\nu/kT}\right)$ = absorption coefficient corrected for induced emission (Z)

$\bar{\mu}^P$ = Planck absorption coefficient (cm^{-1}) (Z)

$K^P = \bar{\mu}^P \tau$ = Planck opacity (cm^2/gm) (Z)

$\bar{\mu}^R$ = Rosseland absorption coefficient (cm^{-1}) (Z, I)

$K^R = \bar{\mu}^R \tau$ = Rosseland opacity (cm^2/gm) (Z, I)

T = material temperature (keV) (Z)

$\varphi = aT^4$ = radiative source function (jerks/ cm^3) (Z)

a = raditation constant (0.0137 jerks/ cm^3/keV^4) (Z)

The Lagrange form of the conservation equations is

Mass Conservation

$$\rho \frac{D}{Dt}(1/\rho) - \bar{\nabla} \cdot \bar{u} = 0 \qquad \text{(A-15)}$$

Momentum Conservation

$$\rho \frac{D}{Dt}\left(\bar{u} + \frac{\bar{F}}{\rho c^2}\right) + \bar{\nabla}\left(P^m + Q\right) + \bar{\nabla} \cdot \left(\bar{\bar{P}}^r - \frac{\bar{u}\bar{F}}{c^2}\right) = 0. \qquad \text{(A-16)}$$

where Q is an artificial viscosity term of the Von Neumann type and $\bar{\bar{P}}^r$ has been defined previously.

Energy Conservation

$$\rho \frac{D}{Dt}\left[\frac{u^2}{2} + \left(E^m + E\right)/\rho\right] + \bar{\nabla} \cdot \left[\bar{F} + \left(P^m + Q - E\right)\bar{u}\right] = W. \qquad \text{(A-17)}$$

Here, W is an energy source in jerks/cm^3/shake, and $u = |\bar{u}|$.

Difference over the k variable will be represented by Δ, i.e., $\Delta = \frac{\partial}{\partial k}$ and

$$\Delta \bar{R}^n_{k+\frac{1}{2},\ell} = \bar{R}^n_{k+1,\ell} - \bar{R}^n_{k,\ell} \qquad \text{(A-18)}$$

Similarly, we use δ for $\frac{\partial}{\partial \ell}$ and

$$\delta \bar{R}^n_{k,\ell+\frac{1}{2}} = \bar{R}^n_{k,\ell+1} - \bar{R}^n_{k,\ell} \qquad \text{(A-19)}$$

A typical zone in k,ℓ space is shown in Fig. A-2 with pressure defined at cell center. There are four artificial viscosities ${}_1q$, ${}_2q$, ${}_3q$, and ${}_4q$ defined along the four sides.

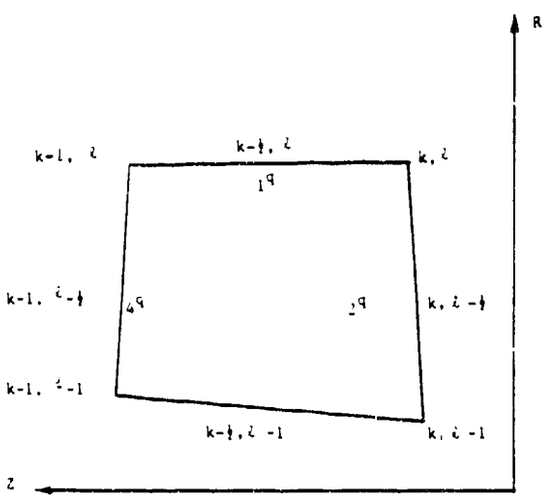

Fig. A-2. Typical Quadrilateral zone in k,ℓ space.

We further break up each zone into four triangles as shown in Fig. A-3. Each of these triangles has an associated material internal energy, E_1, E_2, E_3, E_4, and likewise for the pressure and artificial viscosity.

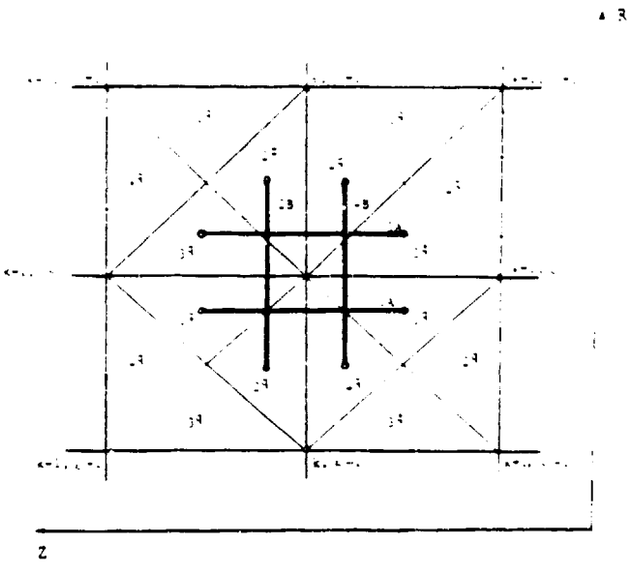

Fig. A-3. Centering of q, p, E with triangular subzone, only ${}_1q$, ${}_2q$, ${}_3q$, and ${}_4q$ are shown.

There are two weighted functions which must be defined for use in the momentum equation. They are obtained as follows. Define

$$\omega_{k+\frac{1}{2},\ell} = \left[\frac{1}{4}\left(\Delta \bar{R}^n_{k+\frac{1}{2},\ell+\frac{1}{2}} + \Delta \bar{R}^n_{k+\frac{1}{2},\ell-\frac{1}{2}}\right)^2\right]^{\frac{1}{2}} \qquad \text{(A-20)}$$

$$\omega_{k,\ell+\frac{1}{2}} = \left[\frac{1}{4}\left(\delta \bar{R}^n_{k+\frac{1}{2},\ell+\frac{1}{2}} + \delta \bar{R}^n_{k-\frac{1}{2},\ell+\frac{1}{2}}\right)^2\right]^{\frac{1}{2}}, \qquad \text{(A-21)}$$

$$\xi'_{k,\ell} = \frac{2\omega_{k-\frac{1}{2},\ell}}{\omega_{k+\frac{1}{2},\ell} + \omega_{k-\frac{1}{2},\ell}}, \qquad \text{(A-22)}$$

$$\eta'_{k,\ell} = \frac{2\omega_{k,\ell-\frac{1}{2}}}{\omega_{k,\ell+\frac{1}{2}} + \omega_{k,\ell-\frac{1}{2}}}. \qquad \text{(A-23)}$$

The weighted functions are then given by

$$\xi_{k,\ell} = \max\left\{0.6, \min\left[\xi'_{k,\ell}, 1.4\right]\right\}, \qquad \text{(A-24)}$$

$$\eta_{k,\ell} = \max\left\{0.6, \min\left[\eta'_{k,\ell}, 1.4\right]\right\}. \qquad \text{(A-25)}$$

Essentially these weighted functions are used to weigh the various pressure difference and artificial viscosity difference terms in the momentum equation based on the proximity of the point of their formation to the point k,ℓ. Actually, it's more of an inverse weight.

The differenced form of the momentum equation without the radiation now becomes

$$\bar{u}^{n+\frac{1}{2}}_{k,\ell} = \bar{u}^{n-\frac{1}{2}}_{k,\ell} + D\bar{u}^{n}_{k,\ell} \tag{A-26}$$

where

$$D\bar{u}^{n}_{k,\ell} =$$

$$Dt^{n}\left\{\eta_{k,\ell}\left[\frac{\partial\bar{\bar{R}}/\partial\ell}{2\rho j}\frac{\partial_1 P}{\partial k}+\frac{1}{2M}\frac{\partial}{\partial k}\left(\hat{R}\frac{\partial\bar{\bar{R}}}{\partial\ell}{}_1q_A\right)\right]^{n}_{k,\ell-\frac{1}{2}}\right.$$

$$-\xi_{k,\ell}\left[\frac{\partial\bar{\bar{R}}/\partial k}{2\rho j}\frac{\partial_2 P}{\partial\ell}+\frac{1}{2M}\frac{\partial}{\partial\ell}\left(\hat{R}\frac{\partial\bar{\bar{R}}}{\partial k}{}_2q_B\right)\right]^{n}_{k-\frac{1}{2},\ell}$$

$$+\left(2-\eta_{k,\ell}\right)\left[\frac{\partial\bar{\bar{R}}/\partial\ell}{2\rho j}\frac{\partial_3 P}{\partial k}+\frac{2}{2M}\frac{\partial}{\partial k}\left(\hat{R}\frac{\partial\bar{\bar{R}}}{\partial\ell}{}_3q_A\right)\right]^{n}_{k,\ell+\frac{1}{2}}$$

$$\left.-\left(2-\xi_{k,\ell}\right)\left[\frac{\partial\bar{\bar{R}}/\partial k}{2\rho j}\frac{\partial_4 P}{\partial\ell}+\frac{1}{2M}\frac{\partial}{\partial\ell}\left(\hat{R}\frac{\partial\bar{\bar{R}}}{\partial k}{}_4q_B\right)\right]^{n}_{k+\frac{1}{2},\ell}\right\} \tag{A-27}$$

The artificial viscosities ${}_1q^n_A$, ${}_3q^n_A$, ${}_2q^n_B$, and ${}_4q^n_B$, appeared in Eq. (A-27) are computed from

$${}_1q^n_A=\frac{1}{2}\left[\frac{3}{4}{}_1q^{n-\frac{1}{2}}_{k-\frac{1}{2},\ell-\frac{1}{2}}+\frac{1}{4}{}_3q^{n-\frac{1}{2}}_{k-\frac{1}{2},\ell-\frac{1}{2}}+\frac{3}{4}{}_1q^{n+\frac{1}{2}}_{k-\frac{1}{2},\ell-\frac{1}{2}}+\frac{1}{4}{}_3q^{n+\frac{1}{2}}_{k-\frac{1}{2},\ell-\frac{1}{2}}\right] \tag{A-28}$$

$${}_3q^n_A=\frac{1}{2}\left[\frac{3}{4}{}_3q^{n-\frac{1}{2}}_{k-\frac{1}{2},\ell-\frac{1}{2}}+\frac{1}{4}{}_1q^{n-\frac{1}{2}}_{k-\frac{1}{2},\ell-\frac{1}{2}}+\frac{3}{4}{}_3q^{n+\frac{1}{2}}_{k-\frac{1}{2},\ell-\frac{1}{2}}+\frac{1}{4}{}_1q^{n+\frac{1}{2}}_{k-\frac{1}{2},\ell-\frac{1}{2}}\right] \tag{A-29}$$

$${}_2q^n_B=\frac{1}{2}\left[\frac{3}{4}{}_2q^{n-\frac{1}{2}}_{k-\frac{1}{2},\ell-\frac{1}{2}}+\frac{1}{4}{}_4q^{n-\frac{1}{2}}_{k-\frac{1}{2},\ell-\frac{1}{2}}+\frac{3}{4}{}_2q^{n+\frac{1}{2}}_{k-\frac{1}{2},\ell-\frac{1}{2}}+\frac{1}{4}{}_4q^{n+\frac{1}{2}}_{k-\frac{1}{2},\ell-\frac{1}{2}}\right] \tag{A-30}$$

$${}_4q^n_B=\frac{1}{2}\left[\frac{3}{4}{}_4q^{n-\frac{1}{2}}_{k-\frac{1}{2},\ell-\frac{1}{2}}+\frac{1}{4}{}_2q^{n-\frac{1}{2}}_{k-\frac{1}{2},\ell-\frac{1}{2}}+\frac{3}{4}{}_4q^{n+\frac{1}{2}}_{k-\frac{1}{2},\ell-\frac{1}{2}}+\frac{1}{4}{}_2q^{n+\frac{1}{2}}_{k-\frac{1}{2},\ell-\frac{1}{2}}\right] \tag{A-31}$$

On the right hand sides of Eqs. (A-28) through (A-31), the artificial viscosities, ${}_1q$, ${}_2q$, ${}_3q$, and ${}_4q$ are located at the center of the triangles as shown in Fig. A-3. The pressure ${}_1P^n$, ${}_2P^n$, ${}_3P^n$, and ${}_4P^n$ appeared in the right hand side of Eq. (A-27), are obtained from the similar formula of ${}_1q^n_A$, ${}_2q^n_B$, ${}_3q^n_A$, and ${}_4q^n_B$ as given by Eqs. (A-28) through (A-31).

DISCLAIMER